nature structural & molecular biology

Article

https://doi.org/10.1038/s41594-025-01691-6

Global analysis of translocon remodeling during protein synthesis at the ER

Received: 13 June 2025

Accepted: 17 September 2025

Published online: 20 October 2025

Check for updates

Arunkumar Sundaram[1,6], Qianru Li[2,6], Yu Wan[3,6], Josephine Tang[4,6], Haoxi Wu[5], Luka Smalinskaitė[5], Ramanujan S. Hegde[5], Zhe Ji[2,3] ✉ & Robert J. Keenan[1] ✉

Protein biogenesis at the endoplasmic reticulum requires translocons comprising the Sec61 protein-conducting channel and several dynamically associated accessory factors. Here we used transcriptome-wide selective ribosome profiling in human cells to monitor cotranslational interactions of accessory factors for N-glycosylation (the OST-A complex) and multipass membrane protein synthesis (the GEL, PAT and BOS complexes). OST-A was preferentially recruited to open Sec61 channels engaged in polypeptide translocation; conversely, GEL, PAT and BOS were recruited synchronously to closed Sec61 channels and stabilized by newly inserted transmembrane domains. Translocon composition changed repeatedly and reversibly during the synthesis of topologically complex multipass membrane proteins. These data establish the molecular logic that underlies substrate-driven translocon remodeling, events that are crucial for the efficient biogenesis of secretory and membrane proteins.

In eukaryotic cells, most secretory and membrane proteins are synthesized on ribosome–translocon complexes (RTCs) at the endoplasmic reticulum (ER)[1]. The central component of this cotranslational translocation machinery is the Sec61 complex, which provides a high-affinity ribosome docking site and forms a membrane-spanning channel[2,3]. The channel can open axially to translocate hydrophilic polypeptide segments into the ER lumen and can open laterally to insert hydrophobic transmembrane domains (TMDs) into the lipid bilayer[4,5].

The 'core translocon' comprises Sec61 and the TRAP complex co-assembled on ribosomes[6,7]. Additional functionality is provided by binding different accessory factors. For example, the 'secretory translocon' additionally contains OST-A, which catalyzes nascent chain N-glycosylation[8–12]. Similarly, the 'multipass translocon' contains the GEL, PAT and BOS complexes, which insert, chaperone and shield TMDs during multipass membrane protein synthesis[13–15]. The rules governing accessory factor assembly and coordination at the core translocon are not well understood but are critical for ensuring accurate protein maturation.

The concept of substrate-driven translocon remodeling was proposed over two decades ago[16]. Recent in vitro studies provided direct experimental support by showing selective recruitment of the GEL, PAT and BOS complexes during synthesis of several model multipass membrane proteins[13,14]. These experiments provided a static view of translocon composition and structure at a small number of defined biogenesis intermediates. Although illuminating, they offer a limited view of translocon remodeling during synthesis of the ~7,000 secretory and membrane protein substrates encoded by the human genome. These substrates vary widely in the number, organization and properties of their TMDs, translocated domains and cytosolic domains. How the machinery dynamically adjusts to handle this diversity is unclear.

Results

Selective ribosome profiling identifies cotranslational clients of OST-A and MPT

To globally define the cotranslational interactions of the OST-A, GEL, PAT and BOS complexes, we used a recently described ribosome

[1]Department of Biochemistry and Molecular Biology, The University of Chicago, Chicago, IL, USA. [2]Department of Pharmacology, Feinberg School of Medicine, Northwestern University, Chicago, IL, USA. [3]Department of Biomedical Engineering, McCormick School of Engineering, Northwestern University, Evanston, IL, USA. [4]Department of Molecular Genetics and Cell Biology, The University of Chicago, Chicago, IL, USA. [5]Cell Biology Division, MRC Laboratory of Molecular Biology, Cambridge, UK. [6]These authors contributed equally: Arunkumar Sundaram, Qianru Li, Yu Wan, Josephine Tang. ✉e-mail: zhe.ji@northwestern.edu; bkeenan@uchicago.edu

https://doi.org/10.1038/s41594-025-01691-6

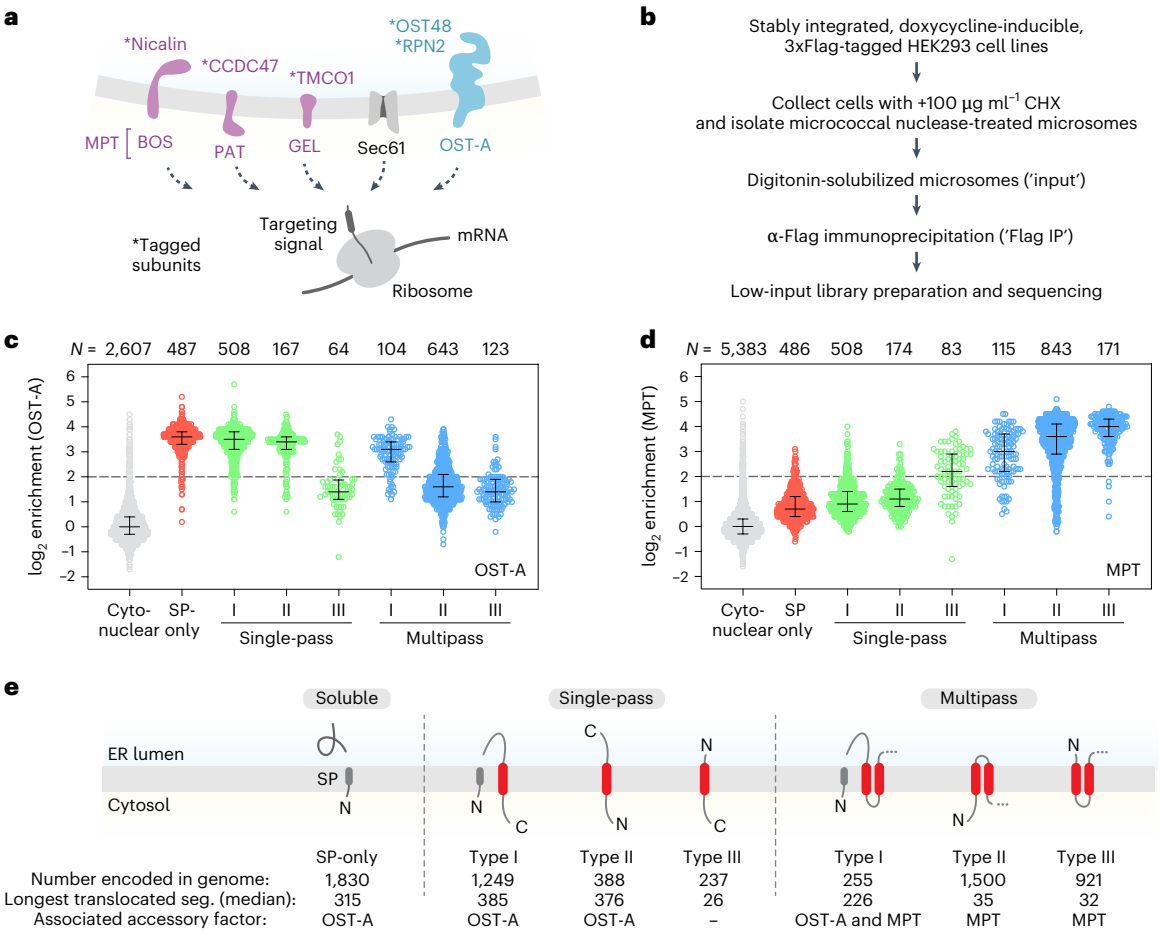

Fig. 1 | Selective ribosome profiling identifies cotranslational clients of the OST-A, GEL, PAT and BOS complexes. a, Individual complexes and their Flag-tagged subunits (marked by asterisks) characterized by selective ribosome profiling. **b**, The sample preparation strategy for low-input ribosome profiling. **c**, OST-A enrichment of transcripts encoding proteins of the indicated type. The enrichment values are calculated as the average of OST48 ($n = 2$) and RPN2 ($n = 1$) samples. The number of sequences (N), median and interquartile range are indicated. **d**, As in **c** but for MPT. The enrichment values are calculated as the average of TMCO1 ($n = 2$), CCDC47 ($n = 2$) and Nicalin ($n = 2$) samples. **e**, Topology cartoons for cotranslational clients of the human ER translocon. The total number of proteins encoded in the human genome, the median length of the longest translocated segment (seg.) and the associated accessory factor are indicated for each class.

profiling method optimized for low-input samples (Fig. 1a,b)[17,18]. Stably integrated HEK293 cell lines expressing near-endogenous levels of Flag-tagged subunits of OST-A (OST48 and RPN2) and the GEL (TMCO1), PAT (CCDC47) and BOS (Nicalin) complexes were constructed, and ribosome-protected mRNA fragments from the total membrane ('input') and affinity-purified fractions ('IP') were prepared and sequenced in biological replicates for each cell line (Extended Data Fig. 1). Enrichment ratios (IP/input) were calculated for each sample by comparative analysis of the two datasets and proteins were annotated using DeepTMHMM[19]. The resulting data were of high quality (Extended Data Figs. 2 and 3), enabling identification of the native clients and corresponding binding sites for each factor.

Transcript enrichment was highly correlated for OST48 and RPN2, as expected for subunits of the same complex, allowing us to combine them into a single sample ($n = 3$), hereafter referred to as 'OST-A' (Extended Data Fig. 3b). Of the ~4,703 proteins detected in the combined dataset, the most enriched ($\log_2 \geq 2$) were proteins with long translocated segments, including signal peptide (SP)-containing soluble secretory proteins ('SP-only', 97%), type I and type II single-pass proteins (96% and 92%, respectively) and type I multipass proteins (88%) (Fig. 1c). Although the GEL, PAT and BOS complexes do not interact with each other in the absence of ribosomes[13], their transcript enrichment (Extended Data Fig. 3b) and interaction profiles (described later) were highly correlated, allowing us to combine them into a single sample ($n = 6$) termed the multipass translocon ('MPT'). Of the ~7,763 proteins detected in the combined MPT dataset, the most enriched ($\log_2 \geq 2$) were membrane proteins with two or more TMDs, including type I (83%), type II (87%) and type III (98%) multipass proteins (Fig. 1d).

Correlation of transcript enrichment with the topologic properties of the different substrate protein classes was consistent with the proposed roles of OST-A and MPT in cotranslational N-glycosylation and multipass membrane protein biogenesis, respectively (Fig. 1e). Substrate classes enriched by OST-A had at least one translocated domain longer than ~100 amino acids, which passes through the Sec61 channel with which OST-A associates[8–11]. Nonenriched classes were cytonuclear proteins or membrane protein classes with few (or no) long translocated segments. By contrast, MPT specifically enriched multipass membrane proteins, whereas cytonuclear proteins, soluble secretory proteins and most single-pass membrane proteins were not enriched[13–15,20].

OST-A engages the translocon during translocation of long segments

Consistent with these topological correlations, analysis of individual interaction profiles revealed that OST-A is selectively recruited during

https://doi.org/10.1038/s41594-025-01691-6

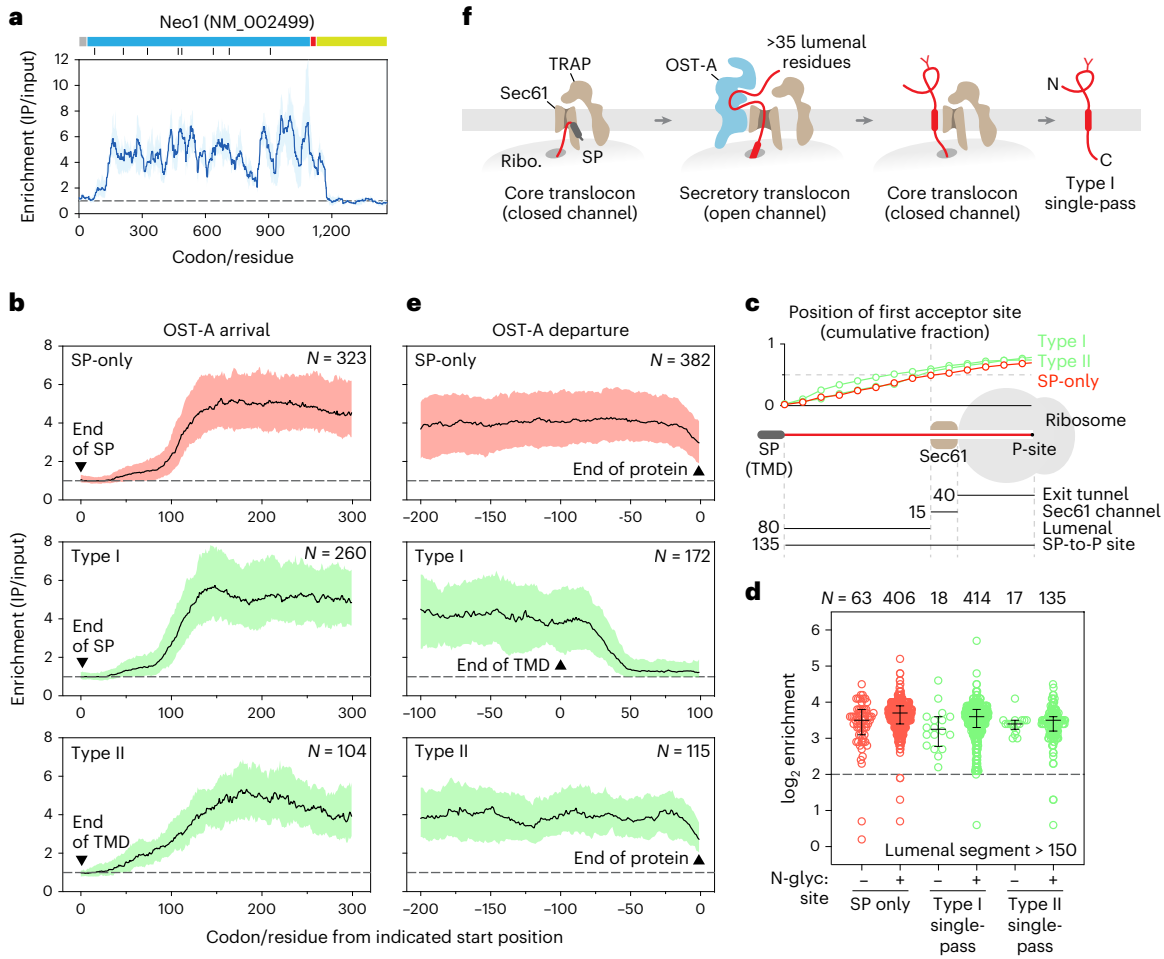

Fig. 2 | OST-A is recruited during translocation of long segments through open Sec61. a, The OST-A interaction profile for Neo1. The mean enrichment (line) and range (shaded) for $n = 3$ replicates are indicated. A diagram of Neo1 is shown above the plot, indicating the signal peptide (gray), lumenal (blue) and cytosolic (yellow) segments, and the single transmembrane domain (TMD) (red). N-glycosylation (N-glyc) acceptor sequences are indicated below by vertical gray lines. This convention is used throughout the manuscript. **b**, Metagene plots of OST-A recruitment to SP-only, type I and type II single-pass proteins, aligned on the end of the indicated feature. The number of sequences (*N*), median and interquartile range are indicated. Only proteins with lumenal segments ≥300 residues are included in the analysis. **c**, The cumulative fraction of proteins whose first N-glycosylation acceptor site (N-X-T/S, X ≠ P) is exposed in the lumen at the point of near-maximal OST-A recruitment (defined as 135 residues past the end of the SP or TMD). **d**, Enrichment scores for SP-only, type I and type II single-pass proteins with or without a lumenal N-glycosylation acceptor site. The number of sequences (*N*), median and interquartile range are indicated. Only proteins with lumenal segments ≥150 residues are included. **e**, Metagene plots of OST-A departure, as in **b**, aligned on the end of the protein (SP-only and type II) or TMD (type I). Only type I proteins with lumenal C-tails ≥100 were included in the analysis. **f**, OST-A arrival and departure during synthesis of a type I single-pass membrane protein at the ribosome (ribo.)-translocon complex.

translocation of long segments. An example is Neogenin (Neo1), a type I single-pass cell surface receptor with eight predicted N-glycosylation acceptor sequences, which recruits OST-A during translocation of its ~1,000-residue extracellular domain (Fig. 2a). Metagene analysis of soluble (SP-only) and type I single-pass proteins, the two most abundant types enriched in the OST samples (Fig. 1c), revealed that OST begins to arrive at the translocon when there are ~90 residues between the end of the signal peptide and the P-site transfer RNA at the peptidyltransferase center (Fig. 2b). A similar but more gradual arrival was observed for type II single-pass proteins. Consistent with previous observations[21], we detected little OST-A binding before this point, even though the ribosome–nascent chain complex is thought to arrive at the membrane earlier, when only ~30–40 residues beyond the first targeting signal have been synthesized[22–24].

Assuming ~55 residues are buried in the ribosome exit tunnel and Sec61 channel, OST-A engagement began when ~35 residues had entered the lumen and was progressively stabilized as translocation continued (Fig. 2b). At these lengths, the nascent chain is long enough to sample the STT3A active site for acceptor sequence N-glycosylation[11,25]. Notably, at a point near maximal OST-A recruitment, when ~80 residues of nascent chain had entered the lumen, the first acceptor site of almost half of all SP-only, type I and type II single-pass proteins was either not yet synthesized or remained buried in the ribosome exit tunnel or Sec61 channel (Fig. 2c). This suggested that OST-A recruitment is insensitive to the presence of an acceptor sequence. Consistent with this, enrichment of SP-only, type I and type II single-pass proteins with long translocated segments was nearly identical whether or not they contained an acceptor sequence (Fig. 2d and Extended Data Fig. 4).

Once recruited to SP-only and type II single-pass proteins, whose C-termini are fully translocated across the membrane, OST-A remained engaged until translation was terminated (Fig. 2e). In contrast, during synthesis of type I single-pass proteins, whose C-termini reside in the cytosol, OST-A departure coincided with emergence of the TMD from the ribosome. Passage of this TMD through the Sec61 lateral gate terminates nascent chain translocation and closes the channel, at which point OST-A disengaged from the translocon (Fig. 2e).

https://doi.org/10.1038/s41594-025-01691-6

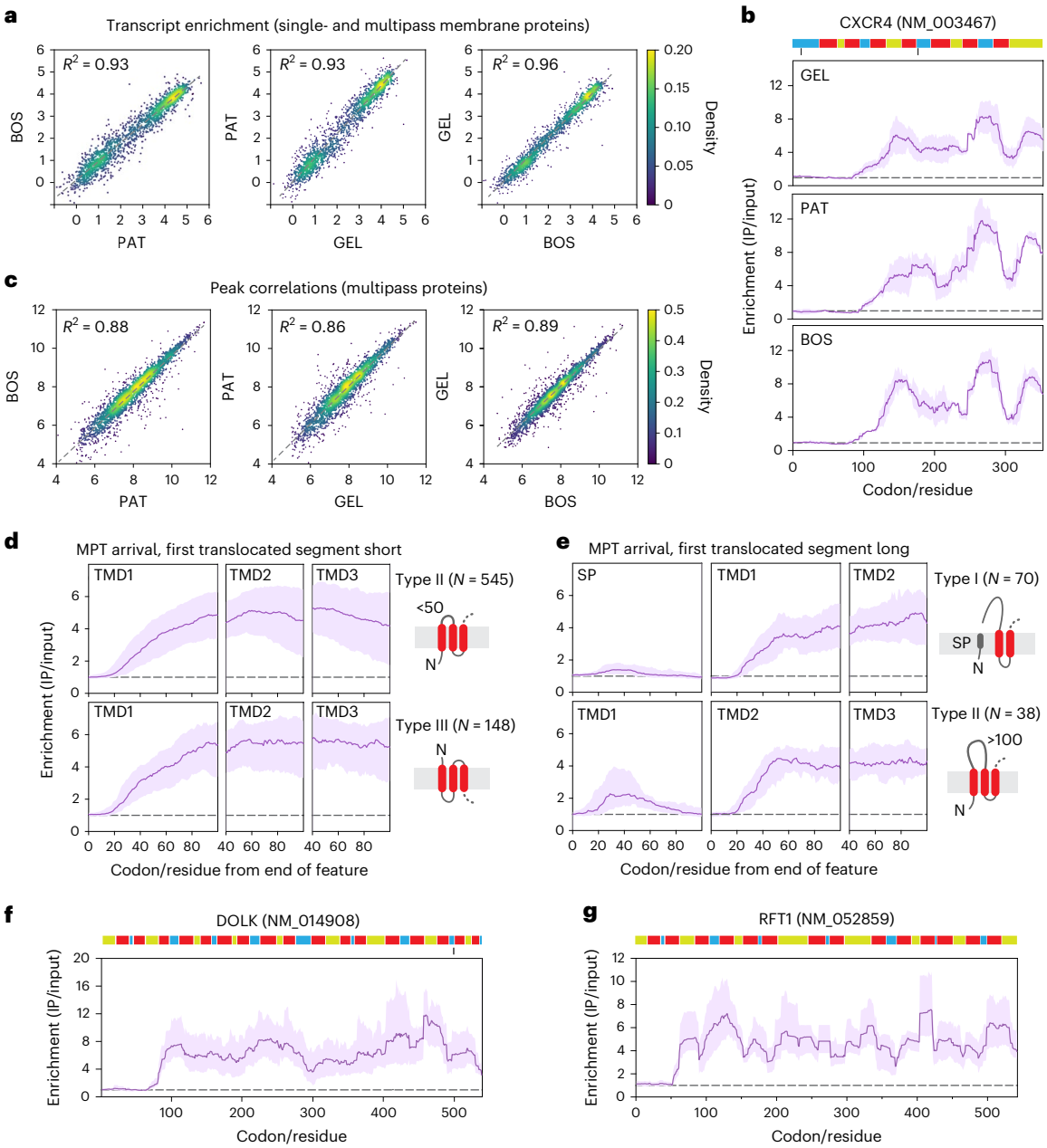

Fig. 3 | Synchronized recruitment of the GEL, PAT and BOS complexes. **a**, Scatter plots of single-pass and multipass membrane protein $\log_2$ transcript enrichment by GEL, PAT and BOS, colored by density. **b**, Interaction profiles for CXCR4. The mean enrichment (line) and range (shaded) for GEL, PAT and BOS ($n = 2$ replicates each) are shown. **c**, Scatter plots of TMCO1, CCDC47 and Nicalin peaks for all multipass proteins, calculated as the sum of enrichment values across each peak (length >10 codons) and colored by density. For peak definition, see Methods. **d**, Metagene plots of MPT ($n = 6$) recruitment to multipass proteins whose first translocated segment is short (≤50 residues), aligned on the end of the indicated feature. The number of sequences (N), median (line) and interquartile range (shaded) are indicated. **e**, As in **d** but for multipass proteins whose first translocated segment is long (≥100 residues). **f**,**g**, MPT interaction profiles for DOLK (**f**) and RFT1 (**g**). The mean enrichment (line) and range (shaded) for $n = 6$ replicates are shown.

Taken together, these data demonstrate that OST-A is not a preassembled translocon component but rather is recruited during translocation of long segments through the open Sec61 channel (Fig. 2f). While OST-A has been observed adjacent to closed Sec61 using a stalled, single-TMD intermediate of a type III substrate prepared in vitro[11], cryo-electron tomography analyses of native secretory translocons in ER membranes show OST-A bound to open Sec61 (refs. 11,26,27). The key structural switch probably involves displacement of the Sec61α plug helix from the center of the channel, which allows it to pack against portions of the Sec61α hinge, Sec61γ and the DC2 subunit of OST-A[27]. The contribution of direct contacts between the nascent chain and the OST-A active site is presumably minor, since nascent chain scanning is necessarily dynamic. Thus, OST-A binding is responsive to the conformation of Sec61—favored during translocation of long segments through the open channel and disfavored when the channel is closed.

Synchronized MPT dynamics at the closed Sec61 channel

The GEL, PAT and BOS complexes can be copurified with ribosomes and Sec61 but do not interact appreciably with each other in the absence of ribosomes[13]. Nevertheless, comparison of the enrichment of transcripts encoding ~2,000 single-pass and multipass membrane

proteins revealed a strong correlation between the three samples, indicating that the GEL, PAT and BOS complexes act on a similar set of clients (Fig. 3a).

Positional analysis revealed that the recruitment dynamics of the GEL, PAT and BOS complexes are also correlated, even though they make only limited contact with each other at the translocon[14]. An example is the C-X-C chemokine receptor type 4 (CXCR4), a type III G-protein-coupled receptor with seven TMDs linked by short hydrophilic segments, which showed nearly identical interaction profiles across its entire length (Fig. 3b). Similar behavior was observed across hundreds of multipass proteins, as shown by the strong correlation between profile peaks for each of the three complexes (Fig. 3c). This agrees with previous in vitro studies on stalled and truncated multipass membrane protein intermediates[13,14].

Earlier in vitro studies showed that recruitment of the GEL, PAT and BOS complexes (MPT) begins when one or more TMDs with a sufficiently long tether to the ribosome enters the membrane[13,14,20]. Metagene analysis of multipass proteins whose first translocated segment was short (<50 residues), including most type II and type III proteins, showed MPT binding was progressively stabilized following emergence of the first TMD or closely spaced TMD pair from the ribosome (Fig. 3d). In contrast, maximal MPT binding was delayed for multipass proteins whose first translocated segment was long (>100 residues), including type I and a subset of type II proteins (Fig. 3e). As discussed later, this was due to nascent chain translocation through open Sec61, which disfavored early MPT binding. With further elongation, translocation was terminated as the downstream TMD passed through the Sec61 lateral gate. This closed the channel and progressively stabilized MPT, which can now bind substrate TMDs in the membrane[13,14,20].

Multipass clients whose downstream lumenal and cytosolic segments are short remained engaged with MPT until translation was complete, regardless of the number of downstream TMDs. Examples of this include DOLK (17 TMDs), RFT1 (14 TMDs), SLC7A11 (12 TMDs) and MFSD3 (12 TMDs) (Fig. 3f,g and Extended Data Fig. 5). Notably, the capacity of the partially enclosed lipid-filled cavity at the center of the MPT is estimated to be ~6–8 TMDs[14,15]. This suggests that TMDs of large multipass proteins can move out of the central cavity during synthesis without disrupting MPT binding.

Interplay between OST-A and MPT during multipass protein synthesis

Of the 866 multipass-encoding transcripts detected in the OST-A and MPT input samples, ~511 were exclusively enriched by MPT affinity purification (Fig. 4a). Nearly all of these encode proteins whose longest translocated segments are short (<50 residues). By contrast, most of the ~268 multipass-encoding transcripts enriched by both OST-A and MPT were found to contain at least one long (>100 residue) translocated segment. These substrates would require the Sec61 channel to remain open during translocation of the long segment[14,28–31].

Positional analysis of transcripts enriched by OST-A and MPT revealed different recruitment patterns depending on the location of the long translocated segment(s). Multipass proteins whose first translocated segment is long, including type I and some (~17%) type II proteins recruited OST-A early, while those whose first translocated segment is short recruited OST-A later (Fig. 4b and Extended Data Fig. 6a,b). Importantly, there was little overlap between OST-A and MPT peaks, consistent with their mutually exclusive binding to the translocon[13,15].

To analyze the early dynamics of OST-A and MPT exchange in more detail, we compared metagene profiles for type I and type II multipass proteins whose first translocated segments are long. Initial MPT sampling of the closed Sec61 channel was disrupted as the signal peptide or first TMD opened Sec61 to initiate translocation (Fig. 4c, left). Subsequently, and similar to the dynamics observed with type I single-pass proteins, OST-A recruitment began when there were ~90 residues between the end of the signal peptide or first TMD and the P-site transfer RNA (~35 residues translocated into the ER lumen) and persisted until translocation was terminated by insertion of the flanking TMD (Fig. 4c, right). At this point, OST-A departed and MPT was stabilized at a presumably closed Sec61.

Once MPT was fully engaged, its continued association depended on the downstream features of the nascent chain. As described above, multipass clients whose downstream lumenal and cytosolic segments are short remained engaged with MPT until translation was complete (Fig. 3f,g). In contrast, synthesis of long, downstream lumenal segments caused MPT to disengage and progressively recruited OST-A as the nascent chain was translocated through Sec61 (Fig. 4d and Extended Data Fig. 6b). A striking example is the Niemann–Pick disease type C intracellular cholesterol transporter 1 protein (NPC1). (Fig. 4e) This heavily glycosylated 1,278-residue type II protein contains 13 TMDs and three long ~250-residue lumenal segments. These segments drive multiple cycles of OST-A and MPT binding and dissociation throughout NPC1 synthesis.

MPT binding was also disrupted during synthesis of long downstream cytosolic segments (Fig. 4f). This is illustrated by HMG-CoA reductase (HMGCR), which binds MPT during synthesis of its eight TMDs before disengaging across a long cytosolic C-tail (Fig. 4g), and the SERCA2 pump (ATP2A2), which alternately engages MPT during TMD synthesis and disengages across two long internal cytosolic loops (Extended Data Fig. 6c). Notably, because these cytosolic segments do not open the Sec61 channel, no OST-A binding is observed.

Different combinations of long lumenal and cytosolic segments give rise to different recruitment patterns (Fig. 4h). A remarkable example is Piezo1, the 2,521-residue pore-forming subunit of the Piezo1 mechanosensitive channel, which contains 38 TMDs, long cytosolic and lumenal domains and several N-glycosylation acceptor sites (Fig. 4i). MPT engaged Piezo1 during periods of closely spaced TMD synthesis and disengaged across long cytosolic and lumenal segments. In contrast, OST-A was recruited during translocation of a 164-residue lumenal segment located between the last two Piezo1 TMDs, but not when MPT disengaged across long cytosolic segments.

Fig. 4 | Interplay between OST-A and MPT during multipass protein synthesis. **a**, An enrichment scatter plot for multipass-encoding transcripts detected in both OST-A and MPT samples, colored according to the length of the longest translocated segment. **b**, OST-A and MPT peak maps for the indicated multipass protein types, sorted by the first MPT peak (length >1% of coding sequence). Each row represents a single transcript normalized by coding region length and colored to indicate positions where either OST-A, MPT or both are enriched. The number (*N*) of each type is indicated. Type II multipass proteins were further classified by the length of the first translocated segment. **c**, Metagene plots of OST-A (blue) and MPT (magenta) recruitment to type I and type II multipass proteins whose first translocated segment is long, aligned on the end of the indicated feature. The median, interquartile range and number of sequences (*N*) are indicated. Only transcripts enriched for OST-A and MPT are included. **d**, Metagene plots of OST-A and MPT dynamics across long (≥100 residue) downstream lumenal segments, aligned to the start of the indicated segment. Only transcripts showing MPT recruitment at the start of the segment were included, and the first translocated segments were excluded from the analysis. The median, interquartile range and number of sequences (*N*) are indicated. **e**, OST-A and MPT interaction profiles for NPC1. The mean enrichment (line) and range (shaded) are shown. **f**, As in **d** but for long downstream cytosolic segments. Only transcripts showing MPT recruitment at the start of the segment were included, and cytosolic N-tails were excluded from the analysis. **g**, OST-A and MPT interaction profiles for HMGCR. The mean enrichment (line) and range (shaded) are shown. **h**, A cartoon illustrating translocon remodeling during synthesis of a hypothetical type 1 multipass protein containing long lumenal and cytosolic segments. **i**, OST-A and MPT interaction profiles for Piezo1. The mean enrichment (line) and range (shaded) are shown.

https://doi.org/10.1038/s41594-025-01691-6

Sec61 is required for translocation of long hydrophilic segments

The substrate enrichment and ribosome profiling analyses indicate that OST-A is preferentially recruited to an open ribosome-bound Sec61 channel, that MPT preferentially favors engagement of a closed Sec61 channel and that the two complexes are mutually exclusive. Furthermore, proteins without any long translocated domains never stably recruit OST-A to the ribosome–Sec61 complex but do, in the case of multipass membrane proteins, recruit and retain MPT. These transcriptome-wide findings are consistent with a recently

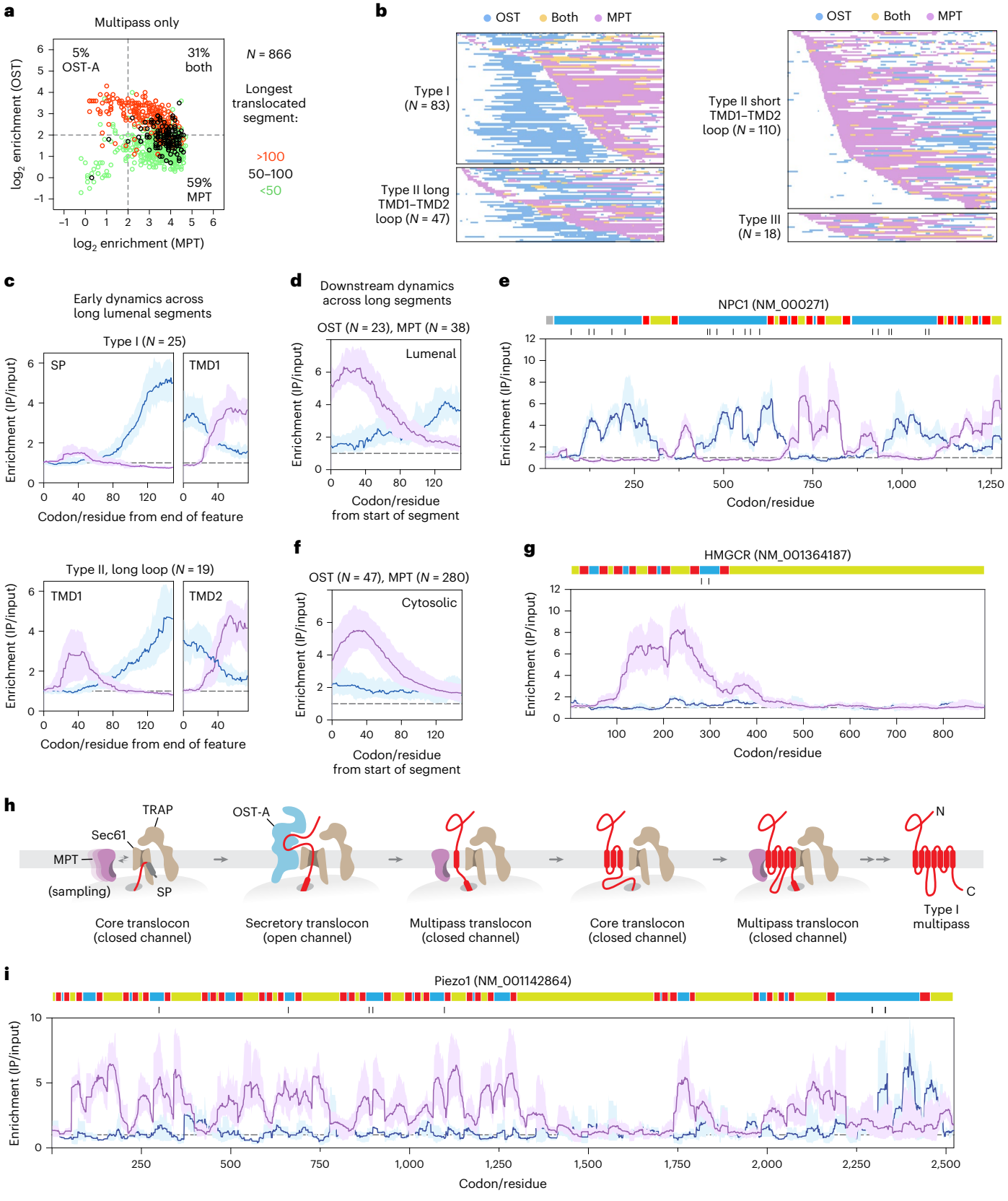

https://doi.org/10.1038/s41594-025-01691-6

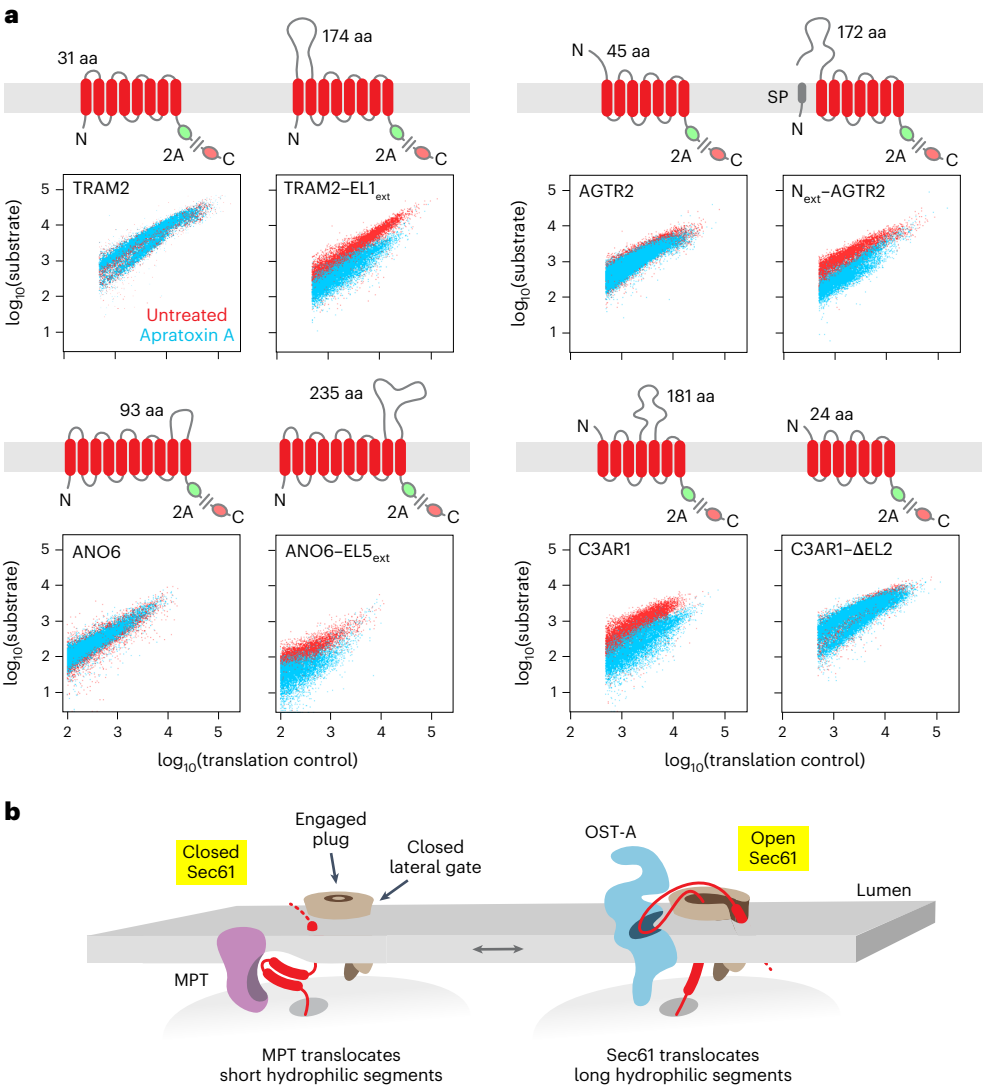

Fig. 5 | Sec61 channel opening is only required for translocation of long hydrophilic segments. a, Topology cartoons and scatter plots for the indicated doxycycline-inducible dual-color reporters expressed by transient transfection in HEK293 cells. Each GFP-tagged substrate is translated in tandem with RFP, separated by a viral P2A sequence that mediates cotranslational ribosome skipping, yielding a GFP-tagged substrate and a free RFP that serves as an internal translation control. Cells were treated during induction with 200 nM ApraA (blue) or dimethylsulfoxide (DMSO) (red) and analyzed by flow cytometry. The length of the longest translocated segment is indicated for each protein. Data are representative of two biological replicates. aa, amino acid; ext, extended. **b**, A model for nascent chain triage between MPT and Sec61.

proposed model for membrane protein insertion in which Sec61 opening is only required for translocation of long segments (>100 residues), whereas an Oxa1 insertase is used for translocation of short segments (<50 residues)[32]. A strong prediction of this model is that classes of substrates where Sec61 is not required to open would be completely refractory to a small-molecule inhibitor of the Sec61 lateral gate that locks Sec61 in a closed configuration.

To test this model in cells, we used a dual-color ratiometric assay for protein stability to monitor the sensitivity of each class of secretory and membrane protein reporters to Apratoxin A (ApraA), a potent small-molecule inhibitor of the Sec61 lateral gate[33] (Fig. 5a and Extended Data Fig. 7a,b). Acute inhibition of Sec61 reduced the stability of every substrate containing at least one long translocated segment. This included a signal peptide-containing secretory protein (EGFP-KDEL), type I single-pass (TREM2 and CD164) and multipass (TM9SF3) membrane proteins, type II single-pass membrane proteins (ASGR1) and a type III multipass protein in which one of the downstream translocated loops was long (C3AR1). By contrast, ApraA had little effect on substrates composed exclusively of short translocated segments, including single-pass type III (CYP4V2) and tail-anchored membrane proteins (VAMP2), and type II and III multipass proteins without long translocated domains (TRAM2, AGTR2 and ANO6).

The sensitivity to ApraA could be directly ascribed to the length of translocated segments because multipass proteins that were insensitive to ApraA (TRAM2, AGTR2 and ANO6) became sensitive when a long translocated segment was introduced (Fig. 5a). Conversely, a sensitive multipass protein (C3AR1) became refractory to inhibition when its long translocated segment was shortened. This result is important because it shows that features of the TMDs, which remain unchanged in all of these constructs, do not determine whether their insertion is via the Sec61 lateral gate. Rather, it is the length of the downstream translocated segment that determines whether the preceding TMD will open the Sec61 channel. These data are consistent with earlier inhibitor studies[14,28–31] and support the model for nascent chain triage between Oxa1 insertases and Sec61 (Fig. 5b).

Discussion

We have analyzed the composition of the ER protein translocation machinery during biogenesis of the secretory and membrane proteome at near-codon resolution. Our results provide a comprehensive view of how and when factors for protein glycosylation (OST-A) and membrane insertion (MPT) engage and disengage from the core Sec61 translocation channel. Several concepts emerge from our findings.

First, OST-A preferentially engages open Sec61 channels that are actively translocating soluble protein domains (with or without N-glycosylation acceptor sequences) into the ER lumen. The mechanism for this probably centers around the Sec61 plug, which is displaced during channel opening to stabilize a network of interactions involving the Sec61α hinge, Sec61γ and the DC2 subunit of OST-A[27]. When translocation is finished and the Sec61 channel closes, this interface is disrupted and OST-A binding is disfavored.

Second, MPT preferentially engages closed Sec61 channels during synthesis of multipass membrane proteins. Recruitment begins at an early stage and is progressively stabilized as TMDs are inserted into the membrane. Once engaged, MPT persists during synthesis of closely spaced TMDs, but disengages over long lumenal segments, probably because of clashes between the PAT complex latch helices and open Sec61 (ref. 14). MPT also disengages over long cytosolic segments. The mechanism for this is not clear, but may reflect accumulation of nascent polypeptide in the limited space at the ribosome-translocon junction[14,15].

Third, the synthesis of many multipass proteins does not require opening of the Sec61 channel. Whereas insertion of TMDs that are followed by long translocated segments requires Sec61, TMDs followed by short translocated segments can be inserted via MPT. Thus, biogenesis of the hundreds of multipass proteins with only short translocated segments can occur without opening the Sec61 channel or engaging OST-A.

Fourth, translocon composition can change repeatedly and reversibly during the synthesis of complex multidomain membrane proteins. At an average elongation rate of 5–10 amino acids per second, it takes about a minute to synthesize a typical 350-residue multipass protein in human cells. This is much slower than the millisecond timescales of protein–protein encounters within the membrane[34]. Thus, the extensive translocon remodeling observed in cells, particularly during synthesis of architecturally complex multipass proteins, is physically reasonable.

Taken together, our data reveal how the nascent polypeptide drives conformational changes in Sec61 that modulate the composition of the translocon. Although exceptions probably exist, these general principles can be extrapolated broadly across the full diversity of the human secretory and membrane proteome.

The observation that type II multipass proteins without long translocated segments are insensitive to ApraA was unexpected since previous work suggested that stalled, single-TMD intermediates derived from these proteins can engage the secretory translocon in vitro[13]. In agreement with the inhibitor data, our profiling analysis showed no evidence for early OST-A recruitment in cells. Translocation of the short segments that connect the first TMD pair of most type II multipass proteins may involve MPT, which begins to sample closed Sec61 channels even before the second TMD has emerged from the ribosome (Fig. 3d), or EMC, which can cotranslationally translocate the short lumenal N-tails of type III multipass proteins[35].

Our data also raise questions about how the already-inserted TMDs of partially synthesized multipass proteins are chaperoned when not sequestered within the MPT central cavity. This can occur in different contexts, including during synthesis of multipass proteins with many TMDs, or when MPT disengages (at least temporarily) from the translocon during synthesis of long cytosolic or lumenal segments. These exposed substrate TMDs would presumably be shielded by general or client-specific intramembrane chaperones such as EMC[36–38], Nacho[39] or other factors. An important future goal will be to identify the relevant chaperones and define how they coordinate with the translocon during multipass protein synthesis.

Online content

Any methods, additional references, Nature Portfolio reporting summaries, source data, extended data, supplementary information, acknowledgements, peer review information; details of author contributions and competing interests; and statements of data and code availability are available at https://doi.org/10.1038/s41594-025-01691-6.

References

1. Rapoport, T. A., Li, L. & Park, E. Structural and mechanistic insights into protein translocation. *Annu. Rev. Cell Dev. Biol.* **33**, 369–390 (2017).
2. Van den Berg, B. et al. X-ray structure of a protein-conducting channel. *Nature* **427**, 36–44 (2004).
3. Gorlich, D. & Rapoport, T. A. Protein translocation into proteoliposomes reconstituted from purified components of the endoplasmic reticulum membrane. *Cell* **75**, 615–630 (1993).
4. Li, L. et al. Crystal structure of a substrate-engaged SecY protein-translocation channel. *Nature* **531**, 395–399 (2016).
5. Voorhees, R. M. & Hegde, R. S. Structure of the Sec61 channel opened by a signal sequence. *Science* **351**, 88–91 (2016).
6. Jaskolowski, M. et al. Molecular basis of the TRAP complex function in ER protein biogenesis. *Nat. Struct. Mol. Biol.* **30**, 770–777 (2023).
7. Pauwels, E. et al. Structural insights into TRAP association with ribosome-Sec61 complex and translocon inhibition by a CADA derivative. *Sci. Adv.* **9**, eadf0797 (2023).
8. Shibatani, T., David, L. L., McCormack, A. L., Frueh, K. & Skach, W. R. Proteomic analysis of mammalian oligosaccharyltransferase reveals multiple subcomplexes that contain Sec61, TRAP, and two potential new subunits. *Biochemistry* **44**, 5982–5992 (2005).
9. Nilsson, I. et al. Photocross-linking of nascent chains to the STT3 subunit of the oligosaccharyltransferase complex. *J. Cell Biol.* **161**, 715–725 (2003).
10. Ruiz-Canada, C., Kelleher, D. J. & Gilmore, R. Cotranslational and posttranslational N-glycosylation of polypeptides by distinct mammalian OST isoforms. *Cell* **136**, 272–283 (2009).
11. Braunger, K. et al. Structural basis for coupling protein transport and N-glycosylation at the mammalian endoplasmic reticulum. *Science* **360**, 215–219 (2018).
12. Pfeffer, S. et al. Structure of the mammalian oligosaccharyl–transferase complex in the native ER protein translocon. *Nat. Commun.* **5**, 3072 (2014).
13. Sundaram, A. et al. Substrate-driven assembly of a translocon for multipass membrane proteins. *Nature* **611**, 167–172 (2022).
14. Smalinskaite, L., Kim, M. K., Lewis, A. J. O., Keenan, R. J. & Hegde, R. S. Mechanism of an intramembrane chaperone for multipass membrane proteins. *Nature* **611**, 161–166 (2022).
15. McGilvray, P. T. et al. An ER translocon for multi-pass membrane protein biogenesis. *eLife* https://doi.org/10.7554/eLife.56889 (2020).
16. Johnson, A. E. & van Waes, M. A. The translocon: a dynamic gateway at the ER membrane. *Annu. Rev. Cell Dev. Biol.* **15**, 799–842 (1999).
17. Li, Q., Stroup, E. K. & Ji, Z. Rfoot-seq: transcriptomic RNase footprinting for mapping stable RNA–protein complexes and rapid ribosome profiling. *Curr. Protoc.* **3**, e761 (2023).
18. Li, Q., Yang, H., Stroup, E. K., Wang, H. & Ji, Z. Low-input RNase footprinting for simultaneous quantification of cytosolic and mitochondrial translation. *Genome Res.* **32**, 545–557 (2022).
19. Hallgren, J. et al. DeepTMHMM predicts alpha and beta transmembrane proteins using deep neural networks. Preprint at *bioRxiv* https://doi.org/10.1101/2022.04.08.487609 (2022).

20. Chitwood, P. J. & Hegde, R. S. An intramembrane chaperone complex facilitates membrane protein biogenesis. *Nature* **584**, 630–634 (2020).
21. Conti, B. J., Devaraneni, P. K., Yang, Z., David, L. L. & Skach, W. R. Cotranslational stabilization of Sec62/63 within the ER Sec61 translocon is controlled by distinct substrate-driven translocation events. *Mol. Cell* **58**, 269–283 (2015).
22. Mothes, W., Prehn, S. & Rapoport, T. A. Systematic probing of the environment of a translocating secretory protein during translocation through the ER membrane. *EMBO J.* **13**, 3973–3982 (1994).
23. Jungnickel, B. & Rapoport, T. A. A posttargeting signal sequence recognition event in the endoplasmic reticulum membrane. *Cell* **82**, 261–270 (1995).
24. Jan, C. H., Williams, C. C. & Weissman, J. S. Principles of ER cotranslational translocation revealed by proximity-specific ribosome profiling. *Science* **346**, 1257521 (2014).
25. Whitley, P., Nilsson, I. M. & von Heijne, G. A nascent secretory protein may traverse the ribosome/endoplasmic reticulum translocase complex as an extended chain. *J. Biol. Chem.* **271**, 6241–6244 (1996).
26. Pfeffer, S. et al. Structure of the native Sec61 protein-conducting channel. *Nat. Commun.* **6**, 8403 (2015).
27. Gemmer, M. et al. Visualization of translation and protein biogenesis at the ER membrane. *Nature* **614**, 160–167 (2023).
28. Hsieh, L. T. et al. The Mycobacterium ulcerans toxin mycolactone causes destructive Sec61-dependent loss of the endothelial glycocalyx and vessel basement membrane to drive skin necrosis. *eLife* https://doi.org/10.7554/eLife.86931 (2025).
29. McKenna, M., Simmonds, R. E. & High, S. Mycolactone reveals the substrate-driven complexity of Sec61-dependent transmembrane protein biogenesis. *J. Cell Sci.* **130**, 1307–1320 (2017).
30. Maifeld, S. V. et al. Secretory protein profiling reveals TNF-α inactivation by selective and promiscuous Sec61 modulators. *Chem. Biol.* **18**, 1082–1088 (2011).
31. Morel, J. D. et al. Proteomics reveals scope of mycolactone-mediated Sec61 blockade and distinctive stress signature. *Mol. Cell. Proteomics* **17**, 1750–1765 (2018).
32. Hegde, R. S. & Keenan, R. J. A unifying model for membrane protein biogenesis. *Nat. Struct. Mol. Biol.* **31**, 1009–1017 (2024).
33. Paatero, A. O. et al. Apratoxin kills cells by direct blockade of the Sec61 protein translocation channel. *Cell Chem. Biol.* **23**, 561–566 (2016).
34. Muller, M. P. et al. Characterization of lipid–protein interactions and lipid-mediated modulation of membrane protein function through molecular simulation. *Chem. Rev.* **119**, 6086–6161 (2019).
35. Chitwood, P. J., Juszkiewicz, S., Guna, A., Shao, S. & Hegde, R. S. EMC is required to initiate accurate membrane protein topogenesis. *Cell* **175**, 1507–1519.e16 (2018).
36. Miller-Vedam, L. E. et al. Structural and mechanistic basis of the EMC-dependent biogenesis of distinct transmembrane clients. *eLife* https://doi.org/10.7554/eLife.62611 (2020).
37. Shurtleff, M. J. et al. The ER membrane protein complex interacts cotranslationally to enable biogenesis of multipass membrane proteins. *eLife* https://doi.org/10.7554/eLife.37018 (2018).
38. Chen, Z. et al. EMC chaperone–Ca_V structure reveals an ion channel assembly intermediate. *Nature* **619**, 410–419 (2023).
39. Hooda, Y. et al. Mechanism of NACHO-mediated assembly of pentameric ligand-gated ion channels. Preprint at *bioRxiv* https://doi.org/10.1101/2024.10.28.620708 (2024).

Methods

Antibodies

Antibodies against human TMCO1 (ref. 40) and Sec61β[41] were characterized previously. Other antibodies were obtained from the following commercial sources: rabbit anti-Nicalin (A305-623A-M) and rabbit anti-CCDC47 (A305-100A) antibodies from Bethyl Laboratories; mouse anti-HRP (ab6728) antibody from Abcam; rabbit anti-peroxidase (SAB3700863) antibody from Sigma; rabbit anti-RPN2 (10576-1-AP) antibody from Proteintech; rabbit anti-uL22 antibody from Abcepta (AP9892b); mouse anti-OST48 (sc-74408) antibody from Santa Cruz Biotechnology; and mouse anti-STT3A (H00003703-M02) antibody from Novus Biologicals. Antibodies were used at 1:1,000 dilution.

Constructs

The following fluorescent reporter constructs were described previously: pcDNA5–GFP–P2A–RFP[35], pcDNA3–mCherry–P2A–Prlss–EGFP–KDEL[42], pcDNA5FRT–GFP–P2A–mCherry–ASGR1 (ref. 35), pcDNA5FRT–GFP–P2A–mCherry–VAMP2 (ref. 43), pcDNA5FRT–TRAM2–GFP–P2A–RFP[35], pcDNA5FRT–AGTR2–GFP–P2A–mCherry[35] and pcDNA5FRT–SS–T4Lysozyme–AGTR2–GFP–P2A–RFP[35]. Additional fluorescent reporter constructs were generated using restriction enzymes or Gibson assembly (New England Biolabs): pcDNA5FRT–HA–TREM2–GFP–P2A–RFP, pcDNA5FRT–HA–CD164–mStayGold–P2A–mCherry, pcDNA5FRT–CYP4V2–GFP–P2A–RFP, pcDNA5FRT–TM9SF3–GFP–P2A–RFP, pcDNA5FRT–TRAM2–extEL1, pcDNA5FRT–ANO6–GFP–P2A–RFP, pcDNA5FRT–ANO6–extEL5, pcDNA5FRT–C3AR1–GFP–P2A–mCherry and pcDNA5FRT–C3AR1ΔEL2–GFP–P2A–mCherry.

Doxycycline-inducible, 3xFlag-tagged OST48, RPN2, TMCO1, CCDC47 and Nicalin constructs were generated by PCR amplification followed by Gibson assembly into pcDNA5/FRT/TO (Thermo Fisher Scientific, V652020). The 3xFlag tags were added at the N-terminus of TMCO1 or inserted after the signal peptide cleavage site for OST48, RPN2, CCDC47 and Nicalin. All constructs were confirmed by DNA sequencing.

Cell culture

Flp-In T-REx 293 cells (Thermo Fisher, R78007) used for flow cytometry analysis were cultured in Dulbecco's modified Eagle medium (DMEM), high glucose, GlutaMAX, pyruvate (Gibco, 10569-010) supplemented with final concentration of 10% FBS (Gibco, 10270106), 10 units ml^{-1} penicillin and 10 μg ml^{-1} streptomycin (Invitrogen, 15070063). All other knockout and stable Flp-In T-REx 293 cell lines were cultured in DMEM (Corning, MT10013CV) supplemented with a 10% FBS (GeminiBio, 900-108), 100 U ml^{-1} penicillin and 100 μg ml^{-1} streptomycin mixture (GeminiBio, 400-109), at 37 °C and 5% CO_2. Cells were checked approximately every 6 months for mycoplasma contamination using the Universal Mycoplasma Detection kit (ATCC, 30-1012 K) and verified to be negative.

Knockout cell line construction

TMCO1, CCDC47 and Nicalin knockout Flp-In T-REx 293 cells were generated by CRISPR–Cas9-mediated gene disruption. Single guide RNAs targeting TMCO1 (5′-GAAACAATAACAGAGTCAGCTGG-3′), CCDC47 (5′-GACAACACAGAAAGTGTGGA-3′) and Nicalin (5′-TCGCTG GGCGCGGACTCCAA-3′) were cloned into pSpCas9(BB)-2A-Puro plasmid (PX459; Addgene #62988), and cells were transfected in a 6-well plate using TransIT-293 (Mirusbio, MIR2700) according to the manufacturer's protocol. After 24 h, cells were selected for 48–72 h with 1 μg ml^{-1} puromycin (InvivoGen, ant-pr-1). Surviving cells were sorted into 96-well plates to obtain single cells, which were then expanded and screened by immunoblotting for successful gene disruption. Knockouts were also validated by PCR amplification of the region of interest from genomic DNA, followed by sequencing and analysis using the Synthego ICE tool.

Stable cell line construction

Stable Flp-In T-REx 293 cell lines containing doxycycline-inducible constructs were generated in the corresponding single knockout (3xFlag–TMCO1, SS_{ER}–3xFlag–CCDC47 and SS_{ER}–3xFlag–Nicalin) or wild-type (SS_{ER}–3xFlag–OST48 and SS_{ER}–3xFlag–RPN2) cell lines, according to the manufacturer's instructions (Thermo Fisher Scientific). Briefly, 100 ng of the desired plasmid were cotransfected with 900 ng of pOG44 (1:9 ratio) in a 6-well plate using TransIT (Mirusbio, MIR2700). After 24 h, cells were selected for Flp-mediated recombination with 100 μg ml^{-1} hygromycin B (Gibco,10687010) for 3–4 weeks to obtain the stably integrated cell lines.

Flow cytometry analysis

Cells were plated into 12-well plates (Corning, 353225) 1 day before transfection. Transfections were performed the next day at 30–50% cell density. For each transfection, 500 ng of indicated plasmids were mixed with 3 μl of TransIT-293 Transfection Reagent (Mirus, MIR 2704) in 100 μl of Opti-MEM (Thermo Fisher, 31985070), incubated at room temperature for 15 min and added dropwise to each well. At 16–24 h later, expression was induced with final concentration of 5 μg ml^{-1} of doxycycline (Sigma, D9891), together with 200 nM of Apratoxin[33] or the same volume of DMSO as a control. Cells were collected 6 h later with 0.6 mM EDTA, pH 7.2 (VWR, 20302.260), washed once with 1× PBS, pH 7.2 and resuspended in 500 μl of FluoroBrite DMEM (Gibco, A18967-01) containing 10% FBS, 10 units ml^{-1} penicillin, 10 μg ml^{-1} streptomycin, 1 mM sodium pyruvate (Gibco, 11360070), 1× GlutaMAX (Gibco, 35050061) and 1 μg ml^{-1} DAPI (Sigma, D9542). Cells were passed through 70 μm cell strainer (Corning, 352350) into analysis tubes (Sarstedt, 55.1579) and analyzed on an LSRFortessa instrument. Signals from a total of at least 10,000 fluorescent and live cells were collected and analyzed on FlowJo 10.10.0. A representative example of the gating strategy is shown in Extended Data Fig. 7a.

Sample preparation for selective ribosome profiling

Cells were seeded in ten 15-cm dishes, induced with 0.5–1.0 ng ml^{-1} doxycycline (MP Biomedicals, 195044) and collected after 72 h (~80% confluency) with ice-cold PBS containing 0.1 mg ml^{-1} cycloheximide (CHX) (Sigma, 01810). Cells were recovered by centrifugation at 2,000*g* for 5 min at 4 °C, washed once with ice-cold PBS containing 0.1 mg ml^{-1} CHX, collected by centrifugation, snap frozen and stored at −80 °C.

Cells were lysed in 9 ml of hypotonic homogenization buffer (10 mM HEPES–KOH pH 7.5, 10 mM KOAc, 1 mM $MgCl_2$ and 0.5× protease inhibitor cocktail (Roche, 11836170001) containing 0.1 mg ml^{-1} CHX for 20 min on ice. Cells were then homogenized by 25 strokes (up and down) in a chilled dounce tissue grinder. Sucrose was added to a final concentration of 250 mM and mixed gently. Nuclei and cell debris were removed by centrifugation at 1,500*g* for 15 min at 4 °C and the supernatant collected. The supernatant fractions were centrifuged again at 1,500*g* for 10 min at 4 °C. The supernatant was collected and centrifuged at 16,500*g* for 15 min at 4 °C. The resulting membrane pellet was resuspended with RTC buffer (50 mM HEPES–KOH pH 7.5, 250 mM sucrose, 250 mM KOAc and 10 mM $MgCl_2$) containing 0.1 mg ml^{-1} CHX to an absorbance at 260 nm (A_{260}) of 50.

Microsomes were treated for 30 min at 37 °C with 5 μl (10,000 U) micrococcal nuclease (NEB, M0247S), 1.25 mM $CaCl_2$ and 0.5 mM phenylmethanesulfonyl fluoride. After micrococcal nuclease treatment, 3 μl (3 U) RNase-free DNase (Promega, M6101) was added and incubated at 5 min at room temperature, followed by quenching with 2.5 mM EGTA. Microsomes were pelleted at 13,500*g* for 10 min at 4 °C. The supernatant was discarded and the membrane pellet was solubilized with RTC buffer supplemented with 2.5% digitonin (Millipore, 300410), 0.1 mg ml^{-1} CHX and 1× protease inhibitor cocktail for 45 min on ice. The digitonin-solubilized material was diluted twice with 150 mM KOAc RTC buffer containing 0.1 mg ml^{-1} CHX and cleared by centrifugation at 16,500*g* for 15 min at 4 °C. The cleared supernatant

(which served as the 'Input' sample for ribosome profiling) (A_{260} ~5) was immunoprecipitated in batch using 50 µl M2 Flag affinity beads (Sigma, A2220) and end-over-end mixing overnight at 4 °C. Flow through was removed and beads were washed four times with 14 column volumes of RTC buffer containing 0.4% digitonin and 0.1 mg ml^{-1} CHX. Bound material was eluted twice, for 30 min on ice, with two column volumes of 200 mM KOAc RTC buffer supplemented with 0.5 mg ml^{-1} Flag peptide (ApexBio, A6001), 0.4% digitonin and 0.1 mg ml^{-1} CHX. The eluate (which served as the 'IP' sample for ribosome profiling) was collected using a pre-equilibrated spin filter column (Thermo Fisher, 69725), snap frozen and stored at −80 °C.

Sucrose gradient

Micrococcal nuclease-treated microsomes were solubilized with low sucrose (50 mM) RTC buffer supplemented with 2.5% digitonin, 0.1 mg ml^{-1} CHX and 1× protease inhibitor cocktail for 30 min on ice. The digitonin-solubilized material was diluted twice with 150 mM KOAc and 50 mM sucrose RTC buffer containing 0.1 mg ml^{-1} CHX and cleared by centrifugation at 16,500*g* for 15 min at 4 °C. The cleared supernatant (A_{260} ~5) was layered onto the top of a 5–50% sucrose gradient prepared in polysome buffer (20 mM Tris pH 7.4, 150 mM NaCl, 5 mM $MgCl_2$ and 1 mM dithiothreitol (DTT)). The gradients were centrifuged in a SW41Ti rotor (Beckman Coulter) in an Optima L-90K ultracentrifuge (Beckman Coulter) at 220,000*g* for 2 h at 4 °C, and then fractionated using a Brandel Density Gradient Fractionation system. The absorbance at 254 nm was monitored with a UV-6 Absorbance Detector and recorded using a built-in chart recorder.

Selective ribosome profiling library preparation using Rfoot-seq

The small amounts of material obtained after immunoprecipitation necessitated the use of a recently developed ribosome profiling protocol (Rfoot-seq) that is optimized for low-input samples[18]. Libraries were generated as described previously[17], with some modifications. After determining the RNA concentration using the Qubit RNA high-sensitivity assay, samples containing an appropriate amount of RNA were digested with optimized RNase conditions to prepare the RNase footprints. For the 'Input' samples, 800–900 ng RNA were digested with 90 U of RNase 1 (LGC Biosearch Technologies, N6901K) in a 95 µl reaction. For 'IP' (purified) samples, 400–800 ng RNA were digested with 40 U of RNase 1 in a 90 µl reaction. The reaction volume was adjusted with lysis buffer (20 mM Tris pH 7.4, 150 mM NaCl, 5 mM $MgCl_2$, 1 mM DTT, 0.1 mg ml^{-1} CHX and 1% v/v Triton X-100). The mixture was incubated at room temperature (25 °C) for 1.5 h with gentle agitation on a nutating mixer. The reaction was quenched by adding 400 µl of TRIzol (Ambion, 15596026), vortexing thoroughly, and then adding 100 µl of chloroform. RNA in the aqueous layer was separated by centrifugation at 12,000*g* for 15 min at 4 °C and precipitated overnight by adding 0.1 volume of 3 M sodium acetate, 10 mg of glycoblue and 1.2 volumes of isopropanol.

Purified RNase footprints were used for library preparation. Footprints were resuspended in 5 µl PNK (NEB, M0201L) reaction mixture (1× PNK buffer, 10 U PNK and 10 U SUPERase·In (Invitrogen, AM2694)) and end repaired at 37 °C for 1 h. Next, 5 µl of polyadenylation mix containing 10 U *E. coli* poly (A) polymerase (NEB, M0276L), 2 µl of 5× first-strand buffer (250 mM Tris−HCl pH 8.3, 375 mM KCl and 15 mM $MgCl_2$), 0.25 mM ATP and 10 U SUPERaseIn was added and the reaction incubated at 37 °C for 2 h. The resulting polyadenylated RNA was then reverse transcribed by a SMART-RT reaction. The reaction mixture was first added with 2.5 µl of reverse transcription primer (10 µM, 5′-ACGTGTGCTCTTCCGATCTNNNNNNNNNNNNNNNTTTTTTTTTTTTTTVN-3′, where 'N' is any base and 'V' is either 'A', 'C' or 'G') and annealed by heating to 72 °C for 5 min and cooled on ice, and then supplemented with SMART-RT mixture (2.5 µl dNTP (10 mM), 400 U Superscript II reverse transcriptase (Invitrogen, 18064014), 10 U SUPERase·In, 4 µl Superscript II first-strand buffer (5×), 1.5 µl DTT (100 mM), 6 µl betaine (5 mM), 0.12 µl $MgCl_2$ (1 M), 0.5 µl template-switching oligos (100 µM 5′-CTCTTTCCCTACACGACG CTCTTCCGATCTNNNNrGrG+G-3′, where 'N' is any base and '+G' is a locked nucleic acid guanylate) and 0.5 µl nuclease-free water. Reverse transcription was carried out with incubation at 42 °C for 1 h, followed by ten cycles of heating at 50 °C for 2 min and then incubating at 42 °C for 2 min. The reverse transcriptase was inactivated by heating at 70 °C for 10 min. RNA footprints hybridized to DNA were removed by incubating at 37 °C for 15 min with 5 U of RNase H (NEB, M0297L). The resultant cDNA was amplified by a first round of PCR with seven cycles, purified and then amplified again in a second round of PCR with four cycles. The DNA library was visualized and separated in a 4% agarose gel. DNA with 15–35-bp insert was excised and recovered using a DNA gel recovery kit (Zymo, D4008). Equal amounts of barcoded libraries were pooled and then sequenced with Illumina NovoSeq.

Rfoot-seq data processing

Reads were trimmed to remove the first seven nucleotides (NNNNGGG) and A-tail adapter sequence using Cutadapt v4.1. Trimmed reads were aligned to ribosomal RNA sequences (5S, NR_023363.1; 5.8S, NR_003285.3; 18S, NR_003286.4; 28S, NR_003287.4) using Bowtie v2.2.6 (ref. 44) allowing up to two mismatches. Unmappable reads were then aligned to the human hg38 genome and RefSeq-defined transcriptome using TopHat v2.1.0 (ref. 45). Uniquely mapped reads were used for downstream analyses.

RibORF[46–48] was used to assess ribosome profiling data quality by examining the read distribution around start and stop codons, checking for 3-nt periodicity and assigning reads to the ribosomal A-site. Two fragment size peaks (19 nt and 28 nt) were observed for all Rfoot-seq samples. Strong 3-nt periodicity was observed for reads with lengths between 18–20 and 26–29 nucleotides, and these reads were selected for further analysis. For each read, genomic location was adjusted to the ribosomal A-site using the offset distance of 15 nt between the 5′-end of the fragment and the A-site.

Gene structure annotation

The hg38 genome sequence and RefSeq-defined transcript annotations were obtained from the UCSC Genome Browser. Where multiple transcript isoforms exist for a gene, the longest coding isoform was selected as the representative isoform. Protein sequences were annotated using DeepTMHMM[19] to predict TMDs and topology. Proteins predicted to contain a signal peptide (SP), but no TMD(s) were defined as SP-only. Proteins with one TMD were defined as single-pass and those with two or more TMDs were defined as multipass. Membrane proteins were further classified as type I, II or III based on predicted topology. Mitochondrial and tail-anchored proteins were removed. Proteins lacking a signal peptide or TMD (cytonuclear) were used as the background gene set for the analyses. A customized Python script was used to identify all N-glycosylation acceptor sequences, N-X-[T/S] (where X ≠ P), located in predicted lumenal segments.

Gene-level expression and enrichment analyses

Gene-level read counts in coding regions were calculated using HTSeq-count v2.0.3 (ref. 49), and transcript per million (TPM) values were used to measure the gene expression level. For each sample, the ratio of TPM values between IP versus input conditions was calculated to indicate the enrichment score. All enrichment scores were $\log_2$ transformed and then subtracted by the median $\log_2$ enrichment score of cytonuclear background genes so that the median of $\log_2$ enrichment scores for background genes was zero. Gene-level enrichment *P* values were calculated for each gene using the chi-square test, comparing the expression levels of a gene versus the median expression of background genes in IP versus input conditions.

The resulting *P* values were corrected for multiple hypothesis testing using the Benjamini–Hochberg procedure.

Positional enrichment analyses across transcripts

Positional enrichment scores were calculated by comparing IP versus input, for each codon in the coding regions. For each A-site-adjusted read in a sample, we first extended the read locations to both ends by 50 nt. Ribosome occupancy at each codon was calculated based on the extended reads measured as the read per million values. The averaged read density across the coding region of a transcript in the input control sample was considered as the base expression level.

The positional enrichment score $E_{i,j}$ for the codon i in the gene j was calculated using the following formula: $E_{i,j} = ((IP_{i,j} + A_j)/B_{IP})/((Input_{i,j} + A_j)/B_{Input}]$, where $IP_{i,j}$ is the read per million value for the codon *i* in the gene *j* in the IP sample and $Input_{i,j}$ is the TPM value for the codon *i* in the gene *j* in the input sample. A_j is the average TPM value across codons for the gene *j* in the input sample. B_{IP} is the sum expression of background cytonuclear genes in the IP sample and B_{Input} is the sum expression of these genes in the input sample. The statistical enrichment *P* value at each codon was calculated by comparing the ratio of the two Poisson rates, using the Python command line 'test_poisson_2indep($IP_{i,j}$, B_{IP}, max($Input_{i,j}$, A_j), B_{Input})'. The resulting *P* values were adjusted for multiple hypothesis testing using the Benjamini–Hochberg procedure.

For metagene enrichment plots, sequences were selected and aligned according to specific criteria, as indicated in the figure legends. At each position, the median and quartiles of $E_{i,j}$ across all genes in an indicated group were calculated and visualized. Interacting regions ('peaks') were defined as continuous stretches of codons with $E_{i,j} > 3$ and an adjusted *P* value $<10^{-3}$. Peaks were extended for codons with $E_{i,j} > 3$ but adjusted *P* value $>10^{-3}$ if they were located within 40 codons of a peak.

Statistics and reproducibility

Rfoot-seq was performed in two biological replicates for Flag–TMCO1, Flag–CCDC47, Flag–Nicalin and Flag–OST48, and a single replicate for Flag–RPN2. Except where noted, the Flag–TMCO1, Flag–CCDC47 and Flag–Nicalin samples were combined into a single sample (called MPT) ($n = 6$). Similarly, Flag–OST48 and Flag–RPN2 were combined into a single sample (called OST-A) ($n = 3$). Flow cytometry experiments were performed at least twice, in biological replicates that showed similar results.

Reporting summary

Further information on research design is available in the Nature Portfolio Reporting Summary linked to this article.

Data availability

Sequencing data are available via the NCBI Gene Expression Omnibus (GEO) repository with accession number GSE297497. Other data are provided in the main text, extended data and Supplementary Information. Materials can be obtained from the corresponding authors upon request. Source data are provided with this paper.

References

40. Anghel, S. A., McGilvray, P. T., Hegde, R. S. & Keenan, R. J. Identification of Oxa1 homologs operating in the eukaryotic endoplasmic reticulum. *Cell Rep.* **21**, 3708–3716 (2017).
41. Fons, R. D., Bogert, B. A. & Hegde, R. S. Substrate-specific function of the translocon-associated protein complex during translocation across the ER membrane. *J. Cell Biol.* **160**, 529–539 (2003).
42. Wang, H. & Hegde, R. S. Identification of a factor that accelerates substrate release from the signal recognition particle. *Science* **386**, 996–1003 (2024).
43. Guna, A., Volkmar, N., Christianson, J. C. & Hegde, R. S. The ER membrane protein complex is a transmembrane domain insertase. *Science* **359**, 470–473 (2018).
44. Langmead, B. & Salzberg, S. L. Fast gapped-read alignment with Bowtie 2. *Nat. Methods* **9**, 357–359 (2012).
45. Kim, D. et al. TopHat2: accurate alignment of transcriptomes in the presence of insertions, deletions and gene fusions. *Genome Biol.* **14**, R36 (2013).
46. Ji, Z., Song, R., Regev, A. & Struhl, K. Many lncRNAs, 5'UTRs, and pseudogenes are translated and some are likely to express functional proteins. *eLife* **4**, e08890 (2015).
47. Ji, Z. RibORF: identifying genome-wide translated open reading frames using ribosome profiling. *Curr. Protoc. Mol. Biol.* **124**, e67 (2018).
48. Yang, H., Li, Q., Stroup, E. K., Wang, S. & Ji, Z. Widespread stable noncanonical peptides identified by integrated analyses of ribosome profiling and ORF features. *Nat. Commun.* **15**, 1932 (2024).
49. Anders, S., Pyl, P. T. & Huber, W. HTSeq—a Python framework to work with high-throughput sequencing data. *Bioinformatics* **31**, 166–169 (2015).

Acknowledgements

This work was supported by NIH grant nos. R35GM145374 (to R.J.K.), R01HL161389 and R35GM138192 (to Z.J.) and MRC MC_UP_A022_1007 (to R.S.H.). J.T. was supported by NIH training grant T32 GM007183.

Author contributions

Conceptualization by A.S., Q.L., Y.W., J.T., Z.J. and R.J.K. Investigation by A.S., Q.L., Y.W., J.T., H.W., L.S., Z.J. and R.J.K. Formal analysis by Y.W. and Z.J. Visualization by Y.W. and R.J.K. Funding acquisition by R.S.H., Z.J. and R.J.K. Supervision by R.S.H., Z.J. and R.J.K. Writing—original draft by R.J.K. Writing—review and editing by A.S., Q.L., Y.W., J.T., H.W., R.S.H., Z.J. and R.J.K.

Competing interests

R.S.H. is a scientific advisor and equity holder of Gate Bioscience. The other authors declare no competing interests.

Additional information

Extended data is available for this paper at https://doi.org/10.1038/s41594-025-01691-6.

Supplementary information The online version contains supplementary material available at https://doi.org/10.1038/s41594-025-01691-6.

Correspondence and requests for materials should be addressed to Zhe Ji or Robert J. Keenan.

Peer review information *Nature Structural & Molecular Biology* thanks Nica Borgese and the other, anonymous, reviewer(s) for their contribution to the peer review of this work. Peer reviewer reports are available. Primary Handling Editor: Katarzyna Ciazynska, in collaboration with the *Nature Structural & Molecular Biology* team.

https://doi.org/10.1038/s41594-025-01691-6

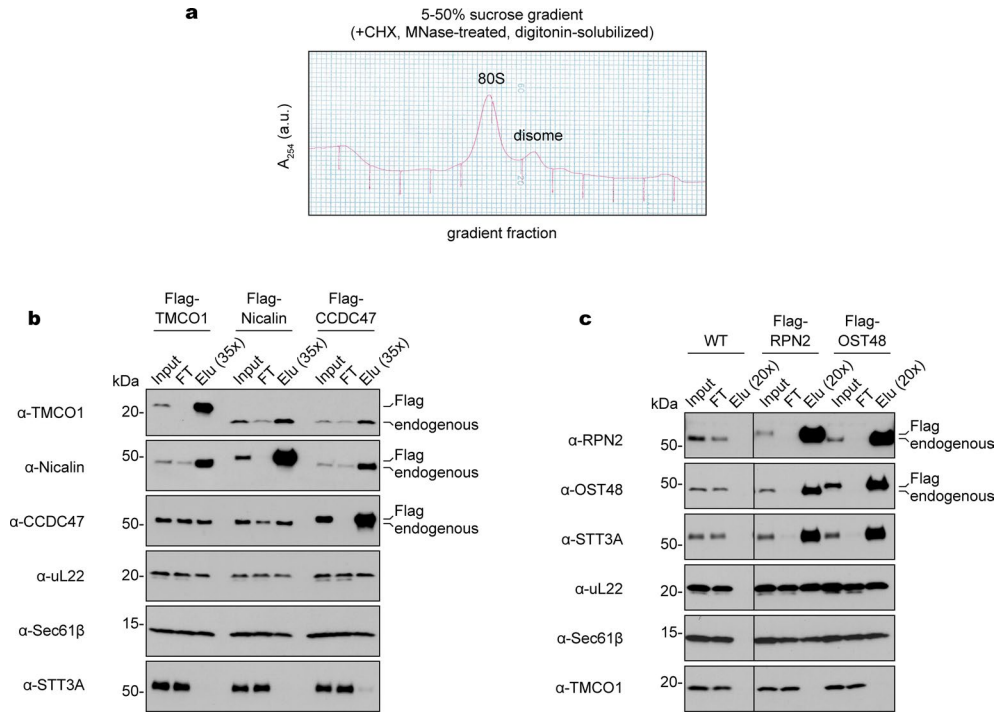

Extended Data Fig. 1 | Sample characterization for selective ribosome profiling. a, Representative example of micrococcal nuclease (MNase)-treated, digitonin-solubilized HEK293 microsomes analyzed on a 5–50% sucrose gradient. **b,c**, Immunoblotting of MNase-treated, digitonin-solubilized microsomes ('input'), and the corresponding flow-through (FT) and elution (Elu) fractions following affinity purification via the indicated Flag-tagged subunit. In each case, the tagged subunit is expressed at roughly the endogenous levels seen in cell lines where that subunit is not tagged. The tagged MPT components are expressed in the corresponding knockout background. The tagged OST-A subunits are expressed in wild-type cells, but in each case the level of the corresponding endogenous protein is low. uL22 is used here as a marker for the ribosome. Data are representative of two biological replicates.

https://doi.org/10.1038/s41594-025-01691-6

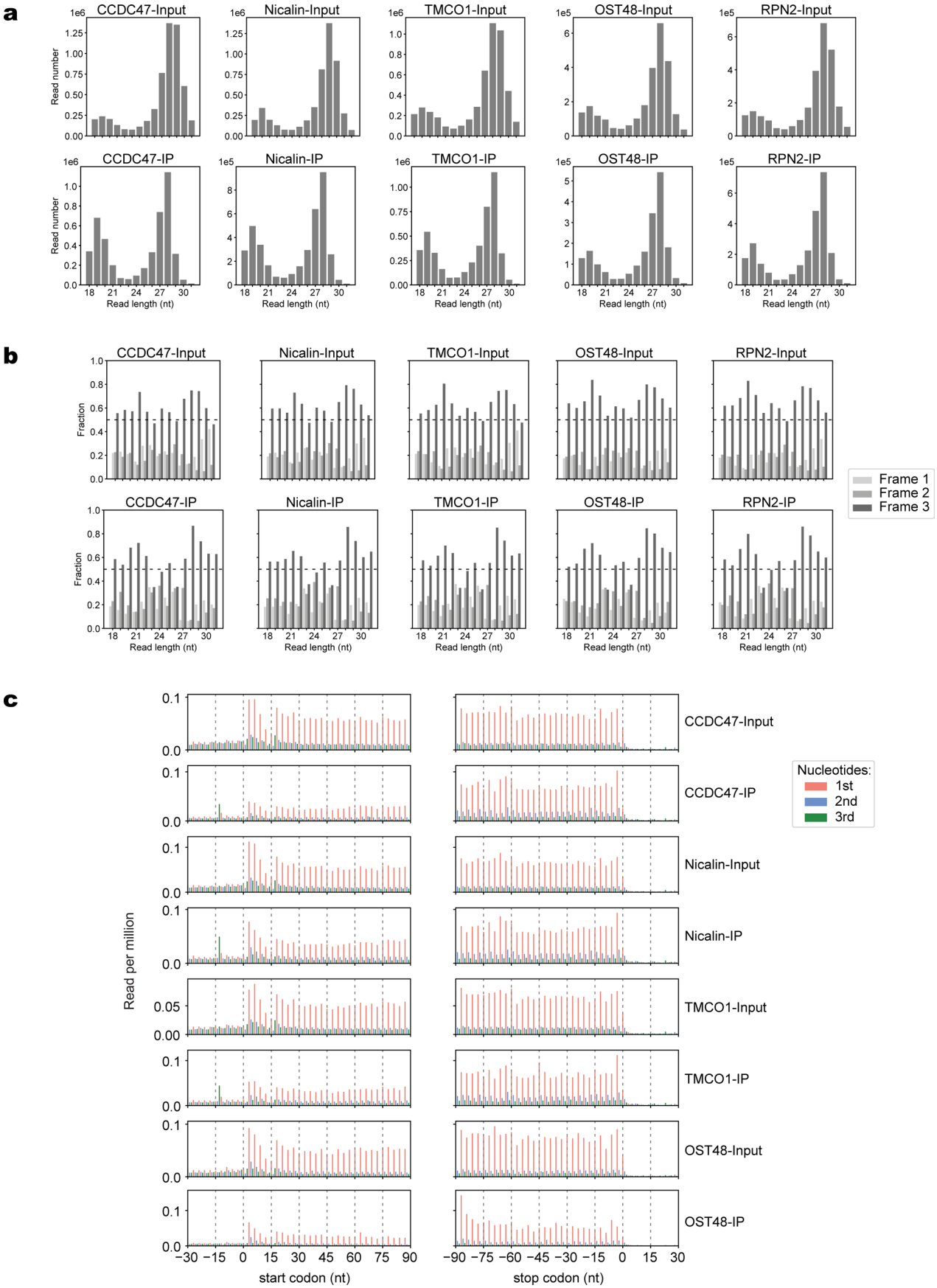

Extended Data Fig. 2 | Quality control of the selective ribosome profiling data. a, Distribution of footprint lengths in coding regions of mRNAs. **b**, Reads were grouped based on footprint lengths (18–35 nt), and the fraction of reads assigned to the three different frames are shown. Strong 3-nt periodicity of read distribution was observed for most footprint sizes. **c**, Ribosomal A-site adjusted read distribution around the start and stop codons of mRNAs.

https://doi.org/10.1038/s41594-025-01691-6

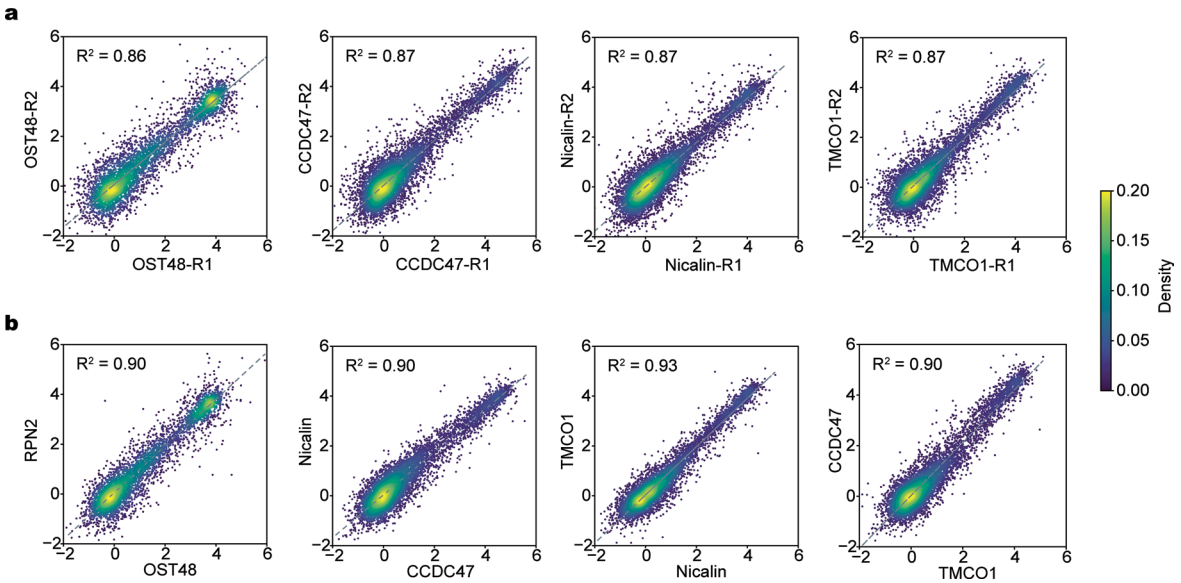

Extended Data Fig. 3 | Comparison of ribosome profiling data for different factors and replicates. a, Scatterplots show the correlation of gene-level enrichment (log2(IP/input)) between two biological replicates for each factor. Each point represents one gene, and all expressed coding genes are included in the analyses. Pearson correlation coefficient values are indicated. **b**, Scatterplots show the correlation of gene-level enrichment (log2(IP/input)) between different factors from the same complexes.

https://doi.org/10.1038/s41594-025-01691-6

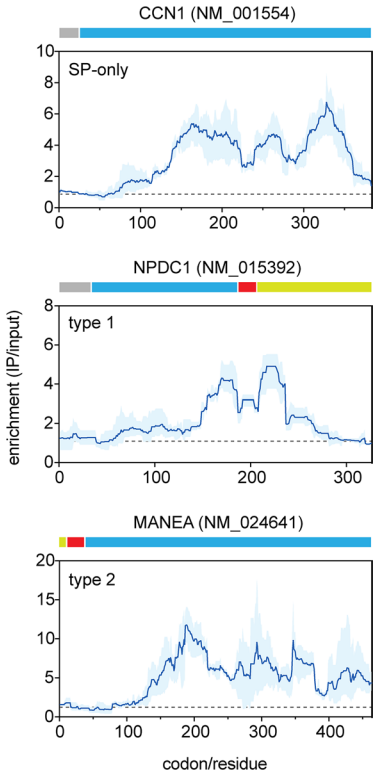

Extended Data Fig. 4 | OST-A recruitment is independent of N-glycosylation acceptor sites. Median (dark blue line) and range (light blue shading) for n = 3 replicates are indicated. Diagrams of CCN1, NPDC1 and MANEA are shown above each plot. Signal peptides (grey), lumenal (blue) and cytosolic (yellow) segments, and transmembrane domains (red) are indicated. Note the robust OST-A recruitment despite the lack of any N-glycosylation acceptor sites in the substrate's lumenal segments.

https://doi.org/10.1038/s41594-025-01691-6

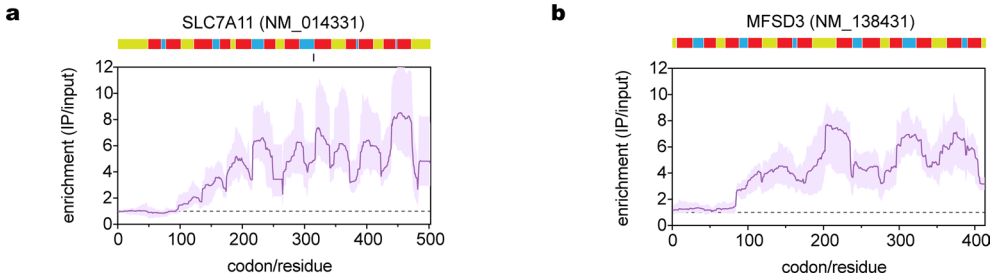

Extended Data Fig. 5 | MPT persistence is independent of the number of TMDs. MPT interaction profiles for **a**, SLC7A11 and **b**, MFSD3. Median (dark magenta line) and range (light magenta shading) for n = 6 replicates are indicated.

https://doi.org/10.1038/s41594-025-01691-6

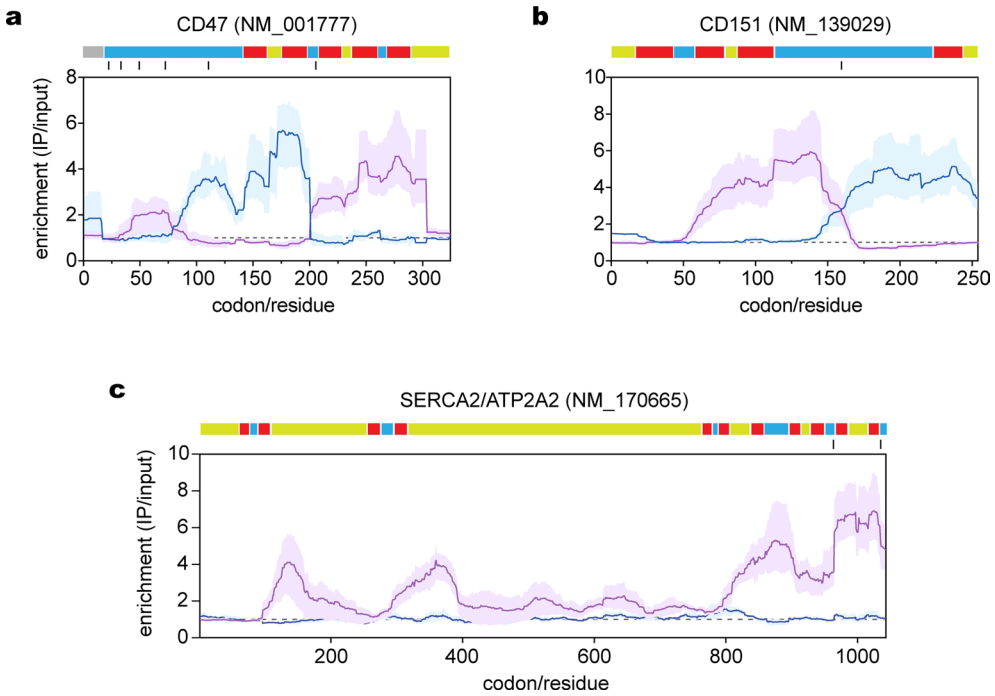

Extended Data Fig. 6 | Additional OST and MPT interaction profiles. MPT (magenta) and OST-A (blue) interaction profiles for **a**, CD47, **b**, CD151, and **c**, the sarco/endoplasmic reticulum calcium ATPase 2 (SERCA2/ATP2A2). Median and range for n = 3 (OST-A) and n = 6 (MPT) replicates are indicated.

https://doi.org/10.1038/s41594-025-01691-6

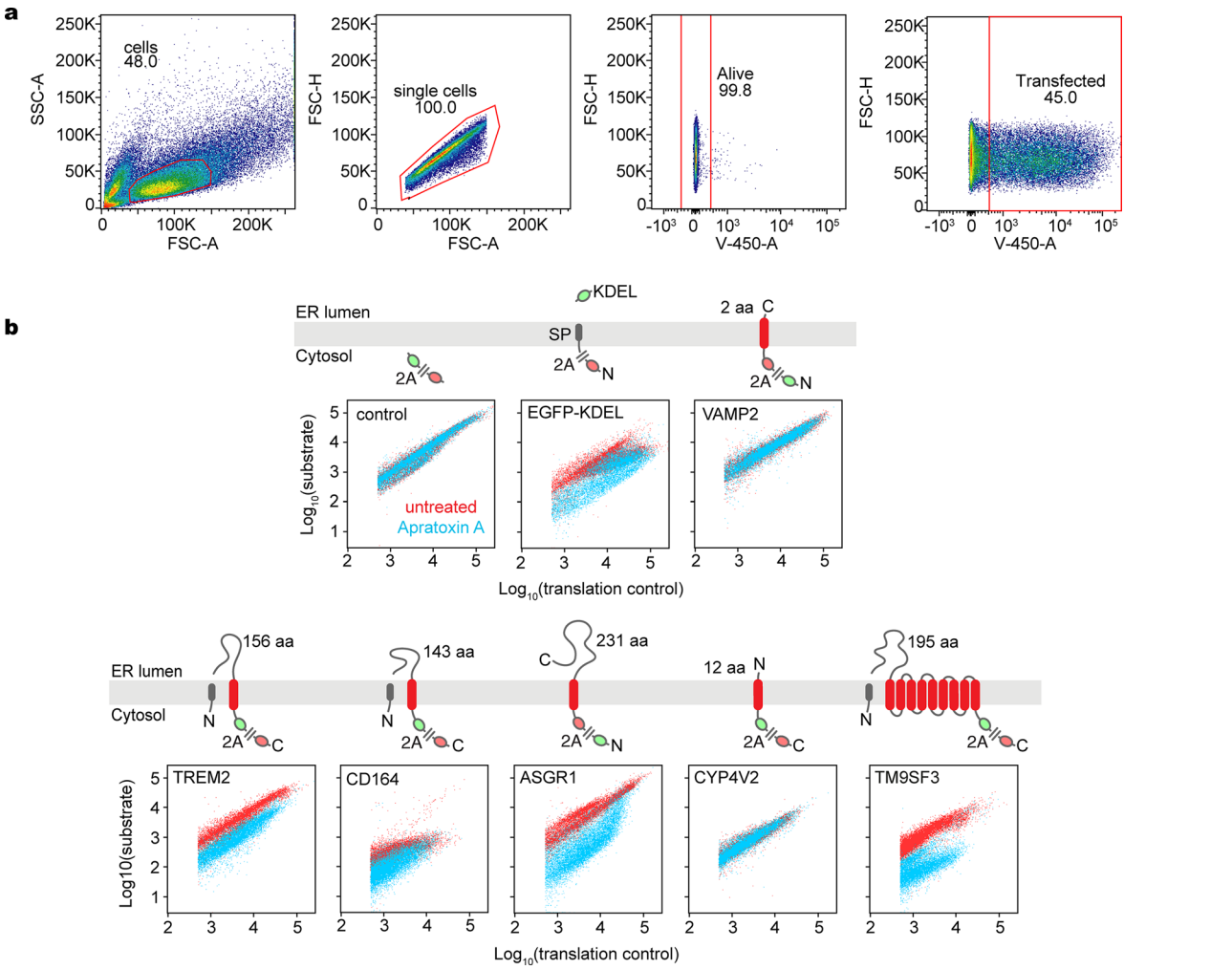

Extended Data Fig. 7 | Effect of Apratoxin A treatment on secretory and membrane protein stability. a, Example of the four-step gating strategy used to analyze dual-color reporters. In step one, forward and side scatter was used to select cells. In step two, height vs. area forward scatter was used to select for single cells. In step three live cells (that is, DAPI-negative) were selected. In step four transfected cells were selected by gating on expression of the translation reporter (GFP or RFP, depending on the construct). Cells meeting all these criteria are plotted in the figures as scatter plots. **b**, Topology cartoons and scatter plots for the indicated doxycycline-inducible dual-color reporters expressed by transient transfection in HEK293 cells. Each fluorescent protein (FP)-tagged substrate is translated in tandem with a different color FP, separated by a viral P2A sequence that mediates cotranslational ribosome skipping. This yields an FP-tagged substrate and a different color FP that serves as an internal translation control. Cells were treated during induction with 200 nM Apratoxin A (blue) or DMSO (red), and analyzed by flow cytometry. The length of the longest translocated segment is indicated for each protein. Data are representative of two biological replicates.

nature portfolio

Corresponding author(s): Zhe Ji, Robert Keenan

Last updated by author(s): 8/20/2025

Reporting Summary

Nature Portfolio wishes to improve the reproducibility of the work that we publish. This form provides structure for consistency and transparency in reporting. For further information on Nature Portfolio policies, see our Editorial Policies and the Editorial Policy Checklist.

Statistics

For all statistical analyses, confirm that the following items are present in the figure legend, table legend, main text, or Methods section.

n/a	Confirmed
☐	☒ The exact sample size (*n*) for each experimental group/condition, given as a discrete number and unit of measurement
☐	☒ A statement on whether measurements were taken from distinct samples or whether the same sample was measured repeatedly
☐	☒ The statistical test(s) used AND whether they are one- or two-sided *Only common tests should be described solely by name; describe more complex techniques in the Methods section.*
☒	☐ A description of all covariates tested
☐	☒ A description of any assumptions or corrections, such as tests of normality and adjustment for multiple comparisons
☐	☒ A full description of the statistical parameters including central tendency (e.g. means) or other basic estimates (e.g. regression coefficient) AND variation (e.g. standard deviation) or associated estimates of uncertainty (e.g. confidence intervals)
☐	☒ For null hypothesis testing, the test statistic (e.g. *F*, *t*, *r*) with confidence intervals, effect sizes, degrees of freedom and *P* value noted *Give P values as exact values whenever suitable.*
☒	☐ For Bayesian analysis, information on the choice of priors and Markov chain Monte Carlo settings
☒	☐ For hierarchical and complex designs, identification of the appropriate level for tests and full reporting of outcomes
☐	☒ Estimates of effect sizes (e.g. Cohen's *d*, Pearson's *r*), indicating how they were calculated

Our web collection on statistics for biologists contains articles on many of the points above.

Software and code

Policy information about availability of computer code

Data collection	N/A
Data analysis	Bowtie v2.2.6; TopHat v2.1.0; HTSeq-count v2.0.3; python 3.10; samtools v1.9; deeptools v3.1.1; DeepTMHMM; RibORF 2.0;

For manuscripts utilizing custom algorithms or software that are central to the research but not yet described in published literature, software must be made available to editors and reviewers. We strongly encourage code deposition in a community repository (e.g. GitHub). See the Nature Portfolio guidelines for submitting code & software for further information.

Data

Policy information about availability of data

All manuscripts must include a data availability statement. This statement should provide the following information, where applicable:

- Accession codes, unique identifiers, or web links for publicly available datasets
- A description of any restrictions on data availability
- For clinical datasets or third party data, please ensure that the statement adheres to our policy

Sequencing data will be available the at the NCBI Gene Expression Omnibus (GEO) repository with accession number GSE297497. All other data are available in the main text or supplementary materials.

Research involving human participants, their data, or biological material

Policy information about studies with human participants or human data. See also policy information about sex, gender (identity/presentation), and sexual orientation and race, ethnicity and racism.

Reporting on sex and gender	N/A
Reporting on race, ethnicity, or other socially relevant groupings	N/A
Population characteristics	N/A
Recruitment	N/A
Ethics oversight	N/A

Note that full information on the approval of the study protocol must also be provided in the manuscript.

Field-specific reporting

Please select the one below that is the best fit for your research. If you are not sure, read the appropriate sections before making your selection.

☒ Life sciences ☐ Behavioural & social sciences ☐ Ecological, evolutionary & environmental sciences

For a reference copy of the document with all sections, see nature.com/documents/nr-reporting-summary-flat.pdf

Life sciences study design

All studies must disclose on these points even when the disclosure is negative.

Sample size	Sample size for each analysis is indicated in figure legends and methods
Data exclusions	One RPN2 replicate failed at the library preparation stage and was discarded.
Replication	Rfoot-seq was performed in two biological replicates for Flag-TMCO1, Flag-CCDC47, Flag-Nicalin, and Flag-OST48, and a single replicate for Flag-RPN2. Except where noted, the Flag-TMCO1, Flag-CCDC47 and Flag-Nicalin samples were combined into a single sample ("MPT") (n=6); similarly, Flag-OST-48 and Flag-RPN2 were combined into a single sample ("OST-A") (n=3). Flow cytometry experiments were performed at least twice, in biological replicates that showed similar results.
Randomization	N/A
Blinding	N/A

Reporting for specific materials, systems and methods

We require information from authors about some types of materials, experimental systems and methods used in many studies. Here, indicate whether each material, system or method listed is relevant to your study. If you are not sure if a list item applies to your research, read the appropriate section before selecting a response.

Materials & experimental systems

n/a	Involved in the study
☐	☒ Antibodies
☐	☒ Eukaryotic cell lines
☒	☐ Palaeontology and archaeology
☒	☐ Animals and other organisms
☒	☐ Clinical data
☒	☐ Dual use research of concern
☒	☐ Plants

Methods

n/a	Involved in the study
☒	☐ ChIP-seq
☐	☒ Flow cytometry
☒	☐ MRI-based neuroimaging

Antibodies

Antibodies used	Antibodies are from the following sources: rabbit anti-TMCO1 (PMID: 29281821); rabbit anti-Sec61β (PMID: 12578908); rabbit anti-Nicalin (A305-623A-M) and rabbit anti-CCDC47 (A305-100A) antibodies from Bethyl Laboratories; mouse anti-HRP (ab6728) antibody from Abcam; rabbit anti-peroxidase (SAB3700863) antibody from Sigma; rabbit anti-RPN2 (10576-1-AP) antibody from Proteintech; rabbit anti-uL22 antibody from Abcepta (AP9892b); mouse anti-OST48 (sc-74408) antibody from Santa Cruz Biotechnology; mouse anti-STT3A (H00003703-M02) antibody from Novus Biologicals. Antibodies were used at 1:1000 dilution.
Validation	Antibodies were validated for specificity against the human antigen by the manufacturer or in earlier published work as follows: Anti-TMCO1 (PMID: 29281821), anti-Nicalin (Bethyl Laboratories) (PMID: 36261522), anti-CCDC47 (Bethyl Laboratories) (PMID: 36261522), anti-STT3A (Novus Biologicals) (PMID: 36261522) and anti-Sec61beta (PMID: 29281821) Anti-RPN2 (Proteintech) and anti-OST48 (Santa Cruz Biotech) were also validated in experiments using tagged cell lines, as described in this manuscript.

Eukaryotic cell lines

Policy information about cell lines and Sex and Gender in Research

Cell line source(s)	Flp-In T-REx 293 cell line are from Invitrogen
Authentication	Flp-In T-REx 293 cell line was authenticated by the antibiotic resistance markers within its genome. All knockouts were validated by PCR amplification of the genomic locus and immunoblotting for the absence of protein.
Mycoplasma contamination	Cells were checked approximately every six months for mycoplasma contamination using the Universal Mycoplasma Detection kit (ATCC), and were found to be negative.
Commonly misidentified lines (See ICLAC register)	None used

Plants

Seed stocks	N/A
Novel plant genotypes	N/A
Authentication	N/A

Flow Cytometry

Plots

Confirm that:

☒ The axis labels state the marker and fluorochrome used (e.g. CD4-FITC).

☒ The axis scales are clearly visible. Include numbers along axes only for bottom left plot of group (a 'group' is an analysis of identical markers).

☒ All plots are contour plots with outliers or pseudocolor plots.

☒ A numerical value for number of cells or percentage (with statistics) is provided.

Methodology

Sample preparation	Samples consisted of Flp-In T-REx 293 cells transiently transfected with the desired reporter construct. Cells were treated with 200 nM of Apratoxin or the same volume of DMSO as a control.
Instrument	LSRFortessa
Software	FlowJo version 10.10.0
Cell population abundance	Signals from a total of at least 10,000 fluorescent and live cells were analysed.

Gating strategy

A four-step gating strategy was used to analyze dual color fluorescent reporters. In step one, forward and side scatter was used to select cells. In step two, height vs. area forward scatter was used to select for single cells. In step three, live cells (i.e., DAPI-negative) were selected. In step four, transfected cells were selected by gating on expression of the translation reporter (GFP or RFP, depending on the construct). Cells meeting all these criteria are plotted in the figures as scatter plots.

☒ Tick this box to confirm that a figure exemplifying the gating strategy is provided in the Supplementary Information.